Dynamic Structure of the Calmodulin-Binding Domain of the Plasma Membrane Ca-ATPase in Native Erythrocyte Ghost Membranes†

Yihong Yao, Jun Gao, and Thomas C. Squier*

Department of Biochemistry, University of Kansas, Lawrence, Kansas 66045-2106

Received April 8, 1996; Revised Manuscript Received June 21, 1996⊗

ABSTRACT: We have used frequency-domain fluorescence resonance energy transfer (FRET) and anisotropy measurements to identify the structural properties of wheat germ calmodulin (CaM) bound to either the plasma membrane Ca-ATPase (PM-Ca-ATPase) in native erythrocyte ghost membranes or a peptide (C25W) that has an identical sequence to the CaM-binding domain on the PM-Ca-ATPase. Cross-linking experiments using benzophenone labeled CaM in conjunction with immunoblots using antibodies specific for either CaM or the PM-Ca-ATPase indicate that one molecule of CaM selectively binds one PM-Ca-ATPase polypeptide chain in native erythrocyte ghost membranes. There are no other proteins in the erythrocyte membrane that bind CaM with high affinity, permitting the measurement of the structural properties of CaM bound to the PM-Ca-ATPase in native erythrocyte ghost membranes. FRET measurements between the fluorophore pyrene maleimide (PMal) located at Cys_{27} in calcium binding loop I and $nitrotyrosine_{139}$ in calcium binding loop IV on wheat germ CaM indicate that the average spatial separation and conformational heterogeneity associated with the two opposing globular domains of CaM are virtually identical upon CaM binding to either the PM-Ca-ATPase or C25W. Measurements of the solvent accessibility and segmental rotational dynamics of PMal-CaM bound to either the PM-Ca-ATPase or C25W further indicate that the local environment around the pyrene label located at Cys_{27} is very similar. However, the overall rotational dynamics of CaM bound to the PM-Ca-ATPase is much slower ($\phi_2 = 83 \pm 14$ ns) than observed when CaM binds C25W ($\phi_2 = 10.3 \pm 0.5$ ns). This implies that CaM is tightly associated with the CaM-binding domain of the PM-Ca-ATPase and that the observed rotational motion of pyrenylmaleimide labeled CaM is characteristic of the global motion of the CaM-binding domain on the PM-Ca-ATPase. The similar conformational heterogeneity and local environment of CaM bound to either the PM-Ca-ATPase or C25W indicates that CaM binds to a contiguous sequence of amino acids on the Ca-ATPase that are analogous to C25W and that there are no significant interactions with other structural elements within the PM-Ca-ATPase. The rate of rotational motion associated with CaM bound to the PM-Ca-ATPase is consistent with hydrodynamic calculations in which the calmodulin-binding domain located at the carboxyl-terminus of the PM-Ca-ATPase has a stable and defined tertiary structure that is independent of the other cytoplasmic domains of the PM-Ca-ATPase.

The plasma membrane Ca-ATPase (PM-Ca-ATPase)[1] belongs to the P-type ion-motive ATPases, which form phosphorylated intermediates involving an aspartic acid during their catalytic cycle (Pederson & Carafoli, 1987a,b). The PM-Ca-ATPase represents the only high affinity calcium transport system present in the plasma membrane of all eukaryotic cells, and functions to maintain the low intracellular calcium levels present in all healthy cells by transporting calcium from the cytosol to the outside of the cell (Carafoli, 1994; James et al., 1995). Calmodulin (CaM) binding activates the PM-Ca-ATPase, which acts both to decrease the free calcium concentration necessary for half-maximal activation of the PM-Ca-ATPase ($K_{Ca^{1}/_{2}}$ decreases from about 20 μM to about 0.5 μM) and to stimulate the maximal velocity of calcium transport activity by more than 2-fold (Jarrett & Penniston, 1977; Niggli et al., 1979). The CaM-binding site on the PM-Ca-ATPase has been identified through the use of a photoaffinity analog of CaM and consists of approximately 30 amino acids near the carboxyl-terminus of the PM-Ca-ATPase, which are highly basic and also have a propensity to form amphipathic α-helices (James et al., 1988; Falchetto et al., 1991; reviewed by Crivici & Ikura, 1995). Cleavage of the CaM-binding domain on the PM-

† Supported by the National Institutes of Health (GM46837) and the American Heart Association.

* Correspondence should be addressed to Thomas C. Squier. Tel: (913)-864-4008; FAX: (913)-864-5321; e-mail: TCSQUIER@KUHUB.CC.UKANS.EDU.

⊗ Abstract published in *Advance ACS Abstracts,* August 15, 1996.

[1] Abbreviations: buffer A, 0.1 M HEPES (pH 7.5), 0.1 M KCl, 1 mM $MgCl_2$, and 0.1 mM $CaCl_2$; Bz, benzophenone-4-maleimide; CaM, calmodulin; CAPS, 3-(cyclohexylamino)-1-propanesulfonic acid; CaMKII, calmodulin-dependent protein kinase II; C25W, a calmodulin target peptide corresponding to the autoinhibitory domain of the plasma membrane Ca-ATPase with the following sequence: QILWFRGLWRIQTQIRVVNAFRSSC (a cysteine was added to the carboxyl terminal of peptide in order to create a fluorescent sensor on the peptide); CSPD, chemiluminescent substrate for alkaline phosphatase; DTNB, 5,5′-dithiobis(2-nitrobenzoic acid); DTT, dithiothreitol; EDTA, ethylenediaminetetraacetic acid; EGTA, ethylene glycol bis(β-aminoethyl ether)-*N*,*N*,*N*′,*N*′-tetraacetic acid; 5F10, mouse monoclonal anti-Ca-ATPase antibody; FRET, fluorescence resonance energy transfer; FURA-2, 1-[[2-(5-carboxyoxazol-2-yl)-6-aminobenzofuran-5-yl]oxy]-2-(2-amino-5-methylphenoxy)ethane-*N*,*N*,*N*′,*N*′-tetraacetic acid; GnHCl, guanidine hydrochloride; HEPES, *N*-(2-hydroxyethyl)piperazine-*N*′-(2-ethansulfonic acid); HPLC, high performance liquid chromatography; PAGE, polyacrylamide gel electrophoresis; PMal, *N*-(1-pyrenyl)-maleimide; PM-Ca-ATPase, the plasma membrane Ca-ATPase; SDS, sodium dodecyl sulfate; TEMPAMINE, 4-amino-2,2,6,6-tetramethyl-1-piperidinyloxyl; TNM, tetranitromethane; ϕ_c, calculated rotational correlation time.

S0006-2960(96)00834-3 CCC: $12.00

Ca-ATPase with either calpain or trypsin results in an equivalent activation of the PM-Ca-ATPase to that observed upon CaM binding (Falchetto et al., 1991). Furthermore, photoaffinity reagents have been used to covalently cross-link exogenously added peptides homologous to the CaM binding sequence of the PM-Ca-ATPase to the calpain truncated and fully active PM-Ca-ATPase, demonstrating a specific structural interaction between the CaM-binding and ATP binding domains of the PM-Ca-ATPase (Falchetto et al., 1992). These results suggest that, in analogy to other CaM-regulated enzymes, the CaM-binding domain of the PM-Ca-ATPase functions as an autoinhibitory domain, and acts to decrease either the accessibility or utilization of the substrates ATP and calcium at the active site of the PM-Ca-ATPase.

General features relating to the predicted topology of the 134 kDa PM-Ca-ATPase indicate an extensive homology to the 110 kDa Ca-ATPase found in skeletal sarcoplasmic reticulum (SR). Two major cytoplasmic domains of the Ca-ATPase contain the ATP binding site and serve to couple the hydrolysis of ATP to the translocation of spatially distant calcium ions associated with the transmembrane helices (reviewed by Inesi et al., 1992; Inesi, 1994; Adebayo et al., 1995; Guerini et al., 1996). The PM-Ca-ATPase contains an additional major cytoplasmic domain that contains about 150 amino acids located at the carboxyl-terminus of the protein. This autoinhibitory domain of the PM-Ca-ATPase contains important regulatory sites associated with the binding of either CaM or acidic phospholipids. Sites within this domain are specifically phosphorylated by either cAMP-dependent protein kinase or protein kinase C (James et al., 1988, 1989; Wang et al., 1991; Rodin et al., 1992; reviewed by Carafoli et al., 1992)

While the physical mechanisms underlying the ability of the autoinhibitory domain on the PM-Ca-ATPase to modulate both the calcium dependence and maximal velocity of the catalytic activity of the PM-Ca-ATPase have not been elucidated, recent work has suggested that interactions between the autoinhibitory domains on adjacent PM-Ca-ATPase polypeptide chains may modulate the transport function of the PM-Ca-ATPase (Kosk-Kosicka & Bzdega, 1988, 1990; Kosk-Kosicka et al., 1990). However, this suggestion has been derived from studies of the associative behavior between PM-Ca-ATPase polypeptide chains in detergent micelles, and is probably not physiologically relevant since the activation of the PM-Ca-ATPase through the association of the autoinhibitory domains on adjacent PM-Ca-ATPase polypeptide chains results in an active species that is independent of CaM (Vorherr et al., 1991; Sackett & Kosk-Kosicka, 1996). Furthermore, while aspects of the structure of CaM bound to a peptide homologous to the CaM-binding sequence in the autoinhibitory domain of the PM-Ca-ATPase indicate that CaM binds to this sequence in an analogous manner to that observed in other CaM-activatable target proteins (Chapman et al., 1992; Yao & Squier, 1996), there is little direct information relating to the structural features of the autoinhibitory domain on the PM-Ca-ATPase in native membranes.

In the present study, we have used fluorescently labeled wheat germ CaM in conjunction with frequency-domain fluorescence spectroscopy (i) to probe the structural properties of the autoinhibitory domain on the PM-Ca-ATPase subsequent to CaM binding in intact erythrocyte ghost membranes, and (ii) to assess the conformation of CaM bound to the PM-Ca-ATPase. These measurements provide the first direct assessment of the conformation and dynamics of the autoinhibitory domain on the PM-Ca-ATPase in intact erythrocyte ghost membranes.

EXPERIMENTAL PROCEDURES

Materials. *N*-(1-Pyrenyl)maleimide (PMal) was obtained from Molecular Probes, Inc. (Junction City, OR). Tetranitromethane (TNM) was obtained from Aldrich (Milwaukee, WI). Nitrocellulose paper was purchased from Millipore (Bedford, MA). Rabbit polyclonal anti-calmodulin antibody was purchased from STI (San Diego, CA). Horseradish peroxidase was purchased from Sigma (St. Louis, MO). Western-light plus chemiluminescent detection system was purchased from Tropix, Inc. (Bedford, MA). Mouse anti-erythrocyte PM-Ca-ATPase monoclonal antibody 5F10 was a gift from Drs. Adelaida G. Filoteo and John T. Penniston (Mayo Clinic). The C25W peptide (QILWFRGLNRIQT-QIRVVNAFRSSC) was synthesized by the Kansas State University Biotechnology Microchemical Core Facility. All other chemicals were the purest grade commercially available. Wheat germ CaM was purified using the procedure outlined by Strasburg et al. (1988) and was found to be greater than 99% pure as assessed by both SDS−PAGE and HPLC. Bovine testes CaM was purified using the procedure outlined by Gopalakrishna and Anderson (1982). Porcine erythrocyte ghosts were prepared essentially as described by Niggli et al. (1979). Purified wheat germ CaM, bovine testes CaM, and erythrocyte ghost membranes were stored at −70 °C. The concentration of C25W peptide was determined using the published extinction coefficient ($\epsilon_{280} = 5600\ M^{-1}\ cm^{-1}$; Chapman et al., 1992).

Specific Derivatization of CaM. The chemical modification of Cys_{27} with *N*-(1-pyrenyl)maleimide (PMal) was carried out essentially as described in Yao et al. (1994), where the specificity of labeling the single cysteine in wheat germ CaM is described in detail. The chemical derivatization of CaM with benzophenone-4-maleimide (Bz) was carried out essentially as described by Strasburg et al. (1988), and DTNB was used to assess the remaining number of unreacted sulfhydryl groups on each CaM. We find approximately 0.90 ± 0.10 mol of Bz incorporated per mole of CaM. Prior to chemical derivatization, CaM was first dissolved in a buffer containing 6 M GnHCl, 25 mM HEPES (pH 7.5), 50 mM DTT, and 1 mM EDTA and incubated at room temperature for 2 h in order to eliminate intermolecular cross-linking. DTT was removed by dialysis against deionized water or with a Sephadex G-25 desalting column (1.6 × 23 cm) prior to lyophilization. The concentration of CaM was determined using the micro BCA assay (Pierce), using a stock solution of desalted bovine CaM whose concentration was determined using the published extinction coefficient for bovine CaM as a standard ($\epsilon_{277} = 3029\ M^{-1}\ cm^{-1}$; Strasburg et al., 1988). Derivatized CaM was stable at −70 °C for at least 2 months, as evidenced by the ability to activate the erythrocyte Ca-ATPase and fluorescence measurements relating to protein structural changes (see Yao et al., 1994). The extent of nitration was measured in 6 M GnHCl, 1 mM EDTA, and 50 mM CAPS (pH 10.0) using the molar extinction coefficient for nitrotyrosine ($\epsilon_{428} = 4200\ M^{-1}\ cm^{-1}$; Richman & Klee, 1978) and corresponds to 0.96 ± 0.06 moles of nitrotyrosine per mole of CaM. Incorporation of Bz was

determined using the published molar extinction coefficient (ϵ_{280} = 13 000 M^{-1} cm^{-1}; Tao et al., 1985) in the presence of 0.1 mM $CaCl_2$ after subtracting the absorbance associated with wheat germ CaM (ϵ_{280} =1565 $M^{-1}cm^{-1}$; Yao et al., 1996).

Preparation of CaM Saturated Ghost Membranes for either Photolysis or Fluorescence Experiments. CaM saturated ghost membranes were prepared by incubating 40 μg (about 2.4 nmol) of either Bz-CaM or fluorescently labeled CaM in the presence of 6.0 mg of porcine erythrocyte ghost membranes (corresponding to about 240 pmol of Ca-ATPase) in a total volume of 1 mL in a buffer composed of 0.1 M HEPES (pH 7.5), 0.1 M KCl, 1 mM $MgCl_2$, and 0.1 mM $CaCl_2$ (buffer A). The mixture was allowed to sit on ice in the dark for 15 min prior to centrifugation at 31000g_{max} for 20 min. The resulting pellet was homogenized and resuspended in the same buffer, and then recentrifuged to remove unbound CaM from the erythrocyte ghost membranes. The pellet was again homogenized and resuspended in buffer A at a final protein concentration of 6 mg mL^{-1}. In the case of the cross-linking experiments, 0.5 mL of the sample was then irradiated at 350 nm using a Rayonet photoreactor for 20 min at 25 °C in a quartz test tube (diameter = 1.5 cm). The sample was then immediately analyzed using SDS−PAGE. In the case of the frequency-domain fluorescence experiments relating to the lifetime and rotational dynamics of CaM, the ghost membranes were resuspended in buffer A at a protein concentration of 0.25 mg mL^{-1}. All preparations were carried out in the dark.

Immunoblotting Experiments. Photolyzed ghost membranes were applied onto SDS−PAGE and then transferred to nitrocellulose paper. Anti-Ca-ATPase and anti-CaM antibodies were used to identify specific interactions between CaM and the PM-Ca-ATPase in the ghost membrane. In the former case, the nitrocellulose paper was incubated with mouse monoclonal anti-Ca-ATPase antibody (5F10), as described by Borke et al. (1989), and the color was developed using the horseradish peroxidase system. In the latter case, the nitrocellulose paper was first incubated with rabbit polyclonal anti-CaM antibody and the positive band was developed with the Western-light plus chemiluminescent detection system, which uses a biotinylated secondary antibody, followed by an anti-biotin streptavidin−alkaline phosphatase conjugate and CSPD, a direct chemiluminescent substrate for alkaline phosphatase, to visualize the rabbit polyclonal antibody.

Enzymatic Analysis. The Ca-ATPase activity of erythrocyte ghosts was determined using the methods described by Lanzetta et al. (1979) for measuring phosphate release. The ghost membrane protein concentration was determined by the method of Biuret (Gornal et al., 1949). The free calcium concentration was calculated using a modified version of the computer program previously described (Fabiato & Fabiato, 1979; Fabiato, 1988), which calculates the multiple equilibria between all ligands in solution. The free calcium concentration was confirmed using 1-[[2-(5-carboxyoxazol-2-yl)-6-aminobenzofuran-5-yl]oxy]-2-(2-amino-5-methylphenoxy)-ethane-*N*,*N*,*N*′,*N*′-tetraacetic acid (FURA-2; λ_{ex} = 340 nm; λ_{em} = 510 nm), as described previously (Yao et al., 1994). The activation of the Ca-ATPase activity upon CaM binding was fit using a simple Langmuir binding isotherm (Matthews, 1993; Pedigo & Shea, 1995), as previously described for the activation of the PM-Ca-ATPase by CaM (Yao et al., 1996).

The free CaM concentration was calculated assuming that 40 pmol of CaM binds to 1 mg of erythrocyte ghost membranes, as discussed in the Results. Therefore:

$$[\mathrm{CaM}]_{free} = [\mathrm{CaM}]_{total} - \left(\left(\frac{\mathrm{ATPase} - \mathrm{ATPase}_0}{\mathrm{ATPase}_{max} - \mathrm{ATPase}_0}\right) \times [\mathrm{Ghosts}] \times 40\ \mathrm{pmol\ mg^{-1}}\right)$$

where ATPase is the observed CaM-dependent ATPase activity, $ATPase_0$ is the basal (CaM-independent) ATPase activity, and $ATPase_{max}$ is the maximum ATPase activity. [Ghosts] is the concentration of erythrocyte ghost membranes in mg mL^{-1}.

Spectroscopic Measurements. Excitation of PMal-CaM involved the 351 nm line from an Innova 400 argon ion laser (Coherent, Santa Clara, CA), and fluorescence detection involved the use of an ISS K2 frequency-domain fluorometer, as described previously (Yao et al., 1994). Steady-state fluorescence emission spectra were measured in the ratio mode using a bandwidth of 4 nm. All measurements involved the detection of the fluorescence emission subsequent to the combination of a Schott GG400 long-pass filter together with an Oriel band-pass filter centered at 420 nm (full width at half-maximum is 10 nm). The sample temperature was maintained at 25 °C.

The measurement of the solvent accessibility of PMal located at Cys_{27} on CaM involved the quenching of the steady-state fluorescence of PMal-CaM (i.e., F/F_0) as a function of the concentration of the spin label TEMPAMINE, where the slope of the line represents the Stern−Volmer quenching constant (K_{sv}; Lehrer & Leavis, 1978). From K_{sv} and the average fluorescence lifetime of the fluorophore ($\bar{\tau}$), one can determine the bimolecular collisional frequency k_q, which is directly related to the solvent exposure of the fluorophore and is calculated by dividing K_{sv} by $\bar{\tau}$.

Decays of Fluorescence Intensities. The lifetime components for PMal-CaM are obtained from the frequency response of the amplitude-modulated light and are characterized by the frequency (ω)-dependent values of the phase shift (ϕ_ω) and the extent of demodulation (m_ω). The parameters describing the decay law are compared with the calculated (c) values ($\phi_{c\omega}$ and $m_{c\omega}$) from an assumed decay law, and the parameters chosen are those that minimize the squared deviation. Explicit expressions have been provided that permit the ready calculation of either the lifetime components relating to a multiexponential decay (i.e., α_i and τ_i; Weber, 1981; Lakowicz et al., 1985) or the distribution of distances between donor and acceptor chromophores for any assumed function (Haas et al., 1978; Beechem & Haas, 1989), as previously described for PMal-CaM (Yao et al., 1994). In either case, the recovered parameters relating to the separation of donor and acceptor chromophores are corrected for the incomplete nitration of $tyrosine_{139}$ (Lakowicz et al., 1991). A distribution of donor−acceptor separations is expected from measurements of molecular dynamics of a range of proteins, as well as statistical mechanical simulations that indicate the conformational heterogeneity associated with long polymers can be adequately described using Gaussian distribution functions (reviewed by Cheung, 1991).

Alternatively, appropriate expressions have been derived permitting the determination of the limiting anisotropy in the absence of rotational diffusion (r_0), the rotational

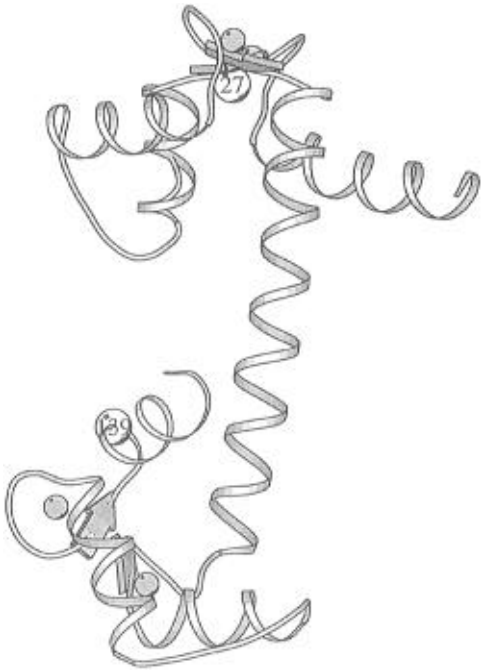

FIGURE 1: Positions of donor and acceptor chromophores within calmodulin. The relative positions of Cys_{27} and Tyr_{139} are highlighted within the tertiary structure of CaM in the ribbon drawing of the backbone fold of the calcium saturated form of CaM. The coordinates are taken from the Brookhaven Protein Data Bank file 1cll.pdb (Chattopadhyaya et al., 1992), and the ribbon drawing was created using MolScript (Kraulis, 1991). Filled circles represent calcium ligands. The model does not attempt to depict known alterations in the tertiary structure of CaM that occur in solution (Török et al., 1992; Yao et al., 1994; reviewed by Crivici & Ikura, 1995).

correlation times (ϕ_i), and the amplitudes of the total anisotropy loss associated with each rotational correlation time ($r_0 g_i$), as previously described in detail (Lakowicz et al., 1985; Lakowicz & Gryczynski, 1991). The parameter values are determined by minimizing the χ_R^2 (the *F* statistic) which serves as a goodness-of-fit parameter that provides a quantitative comparison of the adequacy of different assumed models (Lakowicz & Gryczynski, 1991; Johnson & Faunt, 1992). Data are fit using the method of nonlinear least squares to a sum of exponential decays, using frequency-independent errors ($\delta_{phase} = 0.2°$, $\delta_{mod} = 0.005$; Bevington, 1969).

RESULTS

Fluorescently labeled wheat germ CaM has been used to probe the structure of the autoinhibitory domain of the PM-Ca-ATPase as a result of its unique cysteine and tyrosine residues located near calcium binding sites I and IV, respectively (Figure 1). These amino acids can be covalently modified so as to permit the measurement of the conformation and dynamics of CaM in association with the autoinhibitory domain of the PM-Ca-ATPase. As previously described (Yao et al., 1994), the single Cys_{27} present in calcium binding site I has been covalently modified using *N*-(1-pyrenyl)maleimide (PMal), allowing us to investigate the fluorescence lifetime and rotational dynamics associated with the amino-terminal domain of CaM upon binding to either the PM-Ca-ATPase or a peptide that is homologous to the CaM-binding sequence on the PM-Ca-ATPase (i.e., C25W). The selective nitration of the single Tyr_{139} present

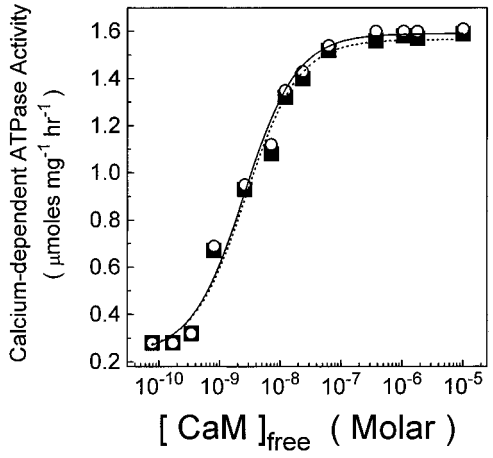

FIGURE 2: CaM stimulation of the erythrocyte ghost PM-Ca-ATPase activity. The CaM dependence of the ATPase activity of porcine erythrocyte PM-Ca-ATPase using wheat germ (■) and bovine testes CaM (○) was fit to a simple Langmuir binding isotherm, as described in the Experimental Procedures. There is a 6.8 ± 0.2 (■) and 6.9 ± 0.2 (○) fold increase in ATPase activity at saturating CaM concentrations, and the corresponding dissociation constants are 2.7 ± 0.4 and 2.6 ± 0.4 nM for wheat and bovine CaM, respectively. ATPase activity was measured at 25 °C in a reaction medium containing 0.4 mg mL^{-1} protein (approximately 16 nM Ca-ATPase) and 3 μM A23187 in buffer A, with a free calcium concentration equal to 30 μM. Measured ATPase activity represents the mean of the two separate experiments and has a standard deviation of 5%.

in calcium binding loop IV permits the measurement of the spatial separation and conformational heterogeneity between PMal and $nitrotyrosine_{139}$ using lifetime-resolved FRET measurements, as described in the Experimental Procedures. Our experimental goal is to use these fluorescence methods to compare the conformation and dynamics of CaM bound to the PM-Ca-ATPase in native erythrocyte ghost membranes with that of CaM bound to a peptide corresponding to the CaM binding sequence on the PM-Ca-ATPase.

Comparison of Biological Activity between Wheat Germ and Bovine CaM. Wheat germ CaM has 90% sequence identity to animal CaM, and in agreement with previous observations (Strasburg et al., 1988) we find that wheat germ and bovine CaM are both able to enhance the catalytic activity of the PM-Ca-ATPase to an equivalent extent and have comparable binding affinities to the PM-Ca-ATPase (Figure 2). Since wheat germ and bovine CaM are indistinguishable with respect to their ability to activate the PM-Ca-ATPase, we are able to use fluorescently labeled wheat germ CaM to assess the structure and dynamics of CaM bound to the CaM-binding domain of the PM-Ca-ATPase. Furthermore, the low basal activity and large activation in the CaM-dependent ATPase activity associated with the PM-Ca-ATPase resulting from the addition of exogenous CaM indicates (i) that there is little endogenous CaM present in our inside-out erythrocyte ghost preparation and (ii) that the majority of the PM-Ca-ATPase in our preparation contains the intact autoinhibitory domain, which functions to inhibit substrate utilization by the calcium pump (reviewed by Carafoli, 1994).

Determination of the Extent of CaM Binding to Porcine Erythrocyte Ghost Membranes. In order to assess the possible specificity of CaM to the PM-Ca-ATPase, we have directly measured the binding capacity of CaM to native erythrocyte ghost membranes. As described in detail in the

Experimental Procedures, native erythrocyte ghost membranes are incubated in the presence of saturating concentrations of CaM, and the unbound CaM was removed through two steps involving the homogenization and centrifugation of the sample. Under these conditions, the high-affinity CaM binding sites associated with the PM-Ca-ATPase are fully saturated, as indicated by the retention of maximal ATPase activity subsequent to the removal of the unbound CaM from the erythrocyte ghost membranes (data not shown). Subsequent to the dissociation of the bound CaM from the erythrocyte membrane upon the addition of 0.1 mM EGTA, we can compare the associated fluorescence of PMal-CaM that was bound to the erythrocyte ghosts to that of known concentrations of PMal-CaM in an analogous buffer. We find that 40 ± 4 pmol of CaM binds per milligram of erythrocyte ghost membranes (data not shown). Previous estimates relating to the concentration of the PM-Ca-ATPase in porcine erythrocyte ghost membranes suggest that the PM-Ca-ATPase accounts for about 0.5% (w/w) of the membrane protein (Knauf et al., 1974; Haaker & Racker, 1979; Bewaji & Bababunmi, 1987; Adamo et al., 1990), or about 37 pmol of PM-Ca-ATPase/mg of erythrocyte ghost protein. Therefore, the binding capacity of the erythrocyte ghost membrane for CaM is consistent with earlier suggestions that the PM-Ca-ATPase represents the only high-affinity CaM binding protein in erythrocyte ghost membranes (Hinds & Andreasen, 1981).

Determination of CaM Binding Proteins in the Erythrocyte Ghosts. It has been previously suggested that CaM can selectively associate with either a 168 kDa protein (that was presumed to be the PM-Ca-ATPase cross-linked with CaM; Hinds & Andreasen, 1981) or spectrin (Husain et al., 1984; Anderson & Morrow, 1987; Yacko et al., 1991) in erythrocyte ghost membranes. Therefore, prior to an examination of the structural properties of CaM in association with proteins in our inside-out erythrocyte ghost membranes, it is critical that we first determine the target protein(s) that bind CaM. We have therefore labeled wheat germ CaM with the photoactivatable cross-linking reagent benzophenone-4-maleimide (Bz) at Cys_{27} (Strasburg et al., 1988; Dormán & Prestwich, 1994). Subsequent to the incubation of erythrocyte ghost membranes with excess Bz-CaM, unbound Bz-CaM is removed by repeated centrifugation as described in the Experimental Procedures. The resulting preparation is exposed to intense ultraviolet light for 20 min, and the resulting products are analyzed using SDS−PAGE (Figure 3). The associated immunoblots using antibodies specific to either the PM-Ca-ATPase (Figure 3B) or CaM (Figure 3C) allow us to visualize the cross-linking product(s) obtained subsequent to the photoactivation of benzophenone.

The Coomassie blue stained gel obtained subsequent to SDS−PAGE does not have sufficient sensitivity to resolve either the PM-Ca-ATPase or the 2 pmol of CaM that is tightly associated with the erythrocyte ghost membranes (Figure 3A). However, it is apparent that our inside-out erythrocyte ghost preparation contains substantially less spectrin (which migrates with apparent molecular masses of about 200 and 220 kDa on SDS−PAGE) than previously observed using preparations developed to investigate the erythrocyte cytoskeleton (Yacko et al., 1991). Immunoblots using antibodies specific for both the PM-Ca-ATPase (i.e., 5F10) and CaM were used to investigate the target protein(s) in erythrocyte ghost membranes that bind CaM with high affinity. The association of Bz-CaM with the PM-Ca-ATPase was assessed in Figure 3B, using the 5F10 antibody

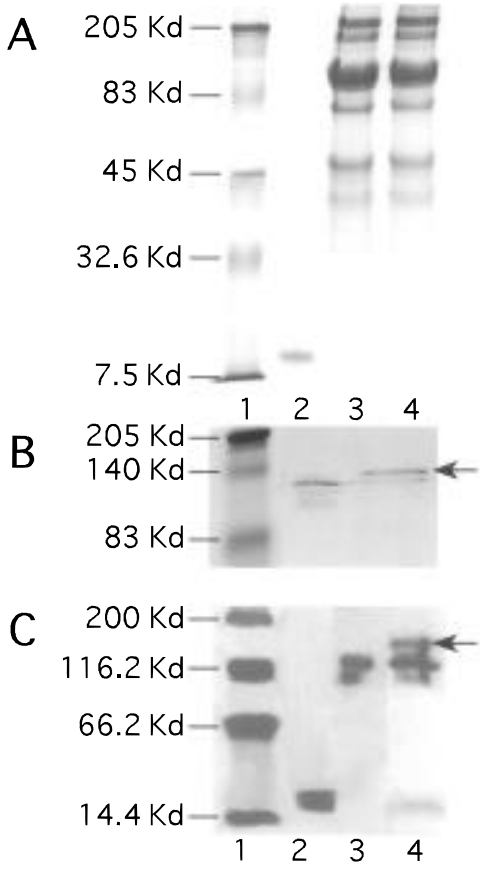

FIGURE 3: Specific interaction between CaM and the PM-Ca-ATPase on the erythrocyte ghosts. (A) 10% acrylamide gel obtained by SDS−PAGE of wheat germ CaM and porcine ghost membranes. SDS−PAGE was performed as described by Laemmli (1970). BioRad's kaleidoscope prestained molecular mass standards are shown in lane 1 with the associated molecular mass and represent myosin (205 kDa), bovine serum albumin (83 kDa) carbonyl anhydrase (45 kDa), soybean trypsin inhibitor (32.6 kDa), and aprotinin (7.5 kDa). Lane 2 is loaded with 2 μg (100 pmol) of wheat germ CaM. Lanes 3 and 4 were loaded with 50 μg of ghost membranes (approximately 2 pmol of PM-Ca-ATPase) in the absence and presence of a saturating amount of added Bz-CaM. (B) Visualization of the PM-Ca-ATPase and its cross-linked product using mouse monoclonal anti-Ca-ATPase antibody following the separation of erythrocyte ghost proteins by SDS−PAGE using a 7−17% continuous polyacrylamide gradient and resulting transfer of the erythrocyte ghost proteins onto nitrocellulose paper by electroblotting. Lane 1 is prestained molecular mass standards and represents myosin (205 kDa), β-galactosidase (140 kDa), and bovine serum albumin (83 kDa). Lanes 2 and 3 are loaded with 50 μg of ghost membranes (approximately 2 pmol of PM-Ca-ATPase) in the absence and presence of saturating amount of Bz-CaM. Lane 2 shows the PM-Ca-ATPase and lane 3 shows the PM-Ca-ATPase, and the cross-linked product between Bz-CaM and PM-Ca-ATPase (indicated by the arrow). (C) Visualization of CaM and its cross-linked product(s) using rabbit polyclonal anti-CaM antibody following the separation of either 0.5 μg (30 pmol) of purified wheat germ CaM (lane 2) or 200 μg of erythrocyte ghost proteins (approximately 7 pmol of the PM-Ca-ATPase) in the absence and presence of saturating amounts of Bz-CaM (lanes 3 and 4, respectively) by SDS−PAGE using a 10% polyacrylamide gel. In lane 4 the arrow indicates the cross-linked product between Bz-CaM and PM-Ca-ATPase. Lane 1 is molecular mass standards and represents myosin (200 kDa), β-galactosidase (116.2 kDa), bovine serum albumin (83 kDa), and lysozyme (14.4 kDa). In all cases the erythrocyte ghost membranes were exposed to ultraviolet light for 20 min in order to activate the benzophenone cross-linking reagent, and unbound CaM was removed prior to cross-linking, as described in the Experimental Procedures.

to visualize the PM-Ca-ATPase. In the absence of added Bz-CaM one observes a major band with an apparent molecular mass of about 134 kDa (corresponding to the intact PM-Ca-ATPase; Strehler et al., 1990) and several smaller bands with apparent molecular masses of about 123 and 113 kDa (Figure 3B, lane 2). The smaller molecular masses may be related to the presence of endogenous proteases in our preparation that cleave the autoinhibitory domain on the PM-Ca-ATPase (James et al., 1989) or as a result of the photolyzing conditions associated with the activation of the Bz cross-linking reagent (see below). However, the smaller molecular mass degradation products associated with the PM-Ca-ATPase are not observed prior to illumination of the sample (data not shown) or subsequent to cross-linking if Bz-CaM is added to the erythrocyte ghost membrane preparation (Figure 3B, lane 3), consistent with the observation that the binding of CaM prevents the proteolytic cleavage of the carboxyl-terminus (which contains the CaM-binding domain) of PM-Ca-ATPase by a range of proteases (Benaim et al, 1984; Zurini et al., 1984).

Subsequent to the addition and photoactivation of Bz-CaM to erythrocyte ghost membranes, a major component is observed with an apparent molecular mass of about 148 kDa (Figure 3B, lane 3, indicated by the arrow) that corresponds to the cross-linked product between Bz-CaM and the PM-Ca-ATPase. Densitometric analysis of the immunoblots indicates that the 148 kDa component corresponds to about 77% of the intensity associated with the immunologically detected proteins that are visualized using the anti-PM-Ca-ATPase antibody. A smaller component with a molecular mass of about 134 kDa accounts for about 23% of the PM-Ca-ATPase protein and corresponds to the PM-Ca-ATPase that was not cross-linked with Bz-CaM (Figure 3B, lane 2). The presence of the 134 kDa band is in good agreement with the observation of a corresponding fraction (about 25%) of Bz-CaM that was not cross-linked to the PM-Ca-ATPase (Figure 3C, lane 4). The observation that most of the Bz-CaM becomes cross-linked to the PM-Ca-ATPase under our photolysis conditions provides strong evidence that under physiological conditions *one molecule of CaM is able to associate with one PM-Ca-ATPase polypeptide chain*.

In order to quantitatively determine the possible presence of other CaM-binding proteins in erythrocyte ghosts in addition to the PM-Ca-ATPase, we have used the Western-light plus chemiluminesent detection system to detect a rabbit polyclonal anti-CaM antibody, which is able to detect cross-linked products between about 1 pmol of CaM and other proteins present in the erythrocyte ghost membrane. As described in the Experimental Procedures, this detection system uses a biotinylated anti-rabbit secondary antibody in conjunction with an anti-biotin streptavidin−alkaline phosphatase conjugate and CSPD to visualize the anti-CaM rabbit polyclonal antibody and, as a result, also detects biotinylated proteins normally present in erythrocyte ghosts. Therefore, prior to the incubation and subsequent cross-linking of Bz-CaM to CaM-binding proteins in erythrocyte ghost membranes, it is first necessary to determine the presence of endogenously biotinylated proteins in erythrocyte ghost membranes. We find two bands with apparent molecular masses of 137 000 and 113 000 Da in our erythrocyte ghost membrane preparation that react with the anti-biotin antibody independent of the addition of exogenous CaM or the anti-CaM antibody (Figure 3C, lane 3). Our erythrocyte ghost preparation contains essentially no endogenous unbound CaM, as indicated by the absence of any lower molecular weight bands that would correspond to CaM (which migrates with an apparent molecular mass of 18 kDa), in agreement with the low basal activity associated with our preparation (Figure 2).

Subsequent to the addition and photoactivatable cross-linking of Bz-CaM to erythrocyte ghost membranes, we observe the appearance of two new bands with apparent molecular masses of 157 and 18 kDa that are observed only subsequent to the inclusion of Bz-CaM prior to photoactivation and subsequent to the incubation of the sample in the presence of anti-CaM antibodies (Figure 3C, lane 4). Quantitation of the relative intensity of the 157 kDa band relative to the 18 kDa band indicates that the 157 kDa band corresponds to about 75% of the CaM in the erythrocyte ghost preparation subsequent to the photoactivation of the Bz-CaM cross-linking reaction. The remaining intensity associated with the 18 kDa band corresponds to free Bz-CaM that is not cross-linked to any membrane components (Figure 3C, lane 1). Furthermore, the relative molar ratio between the 157 kDa band and the 18 kDa band is virtually the same as the observed molar ratio between the bands corresponding to the Bz-CaM cross-linked PM-Ca-ATPase and the PM-Ca-ATPase that is observed using the anti-PM-Ca-ATPase antibody (Figure 3B, lane 3). The absence of any other species than the PM-Ca-ATPase in association with CaM suggests that no other proteins in our erythrocyte ghost membrane preparation bind CaM to an appreciable extent with high affinity. The differences in the apparent molecular weights of the cross-linked product between Bz-CaM and the PM-Ca-ATPase observed using anti-PM-Ca-ATPase antibodies (Figure 3B, lane 3) and anti-CaM antibodies (Figure 3C, lane 4) are related to differences in the relative mobility of the PM-Ca-ATPase on these different gel systems, which use different concentrations of acrylamide. Since each CaM associates with a single PM-Ca-ATPase polypeptide chain, it is furthermore evident that there is about 40 ± 4 pmol of PM-Ca-ATPase/mg of erythrocyte ghost membrane. Since the PM-Ca-ATPase has a molecular mass of 134 kDa, this implies that about 0.5% of the membrane protein in the erythrocyte ghost membrane preparation corresponds to the PM-Ca-ATPase, in good agreement with earlier estimations (Knauf et al., 1974; Haaker & Racker, 1979; Bewaji & Bababunmi, 1987; Adamo et al., 1990).

In addition to the biotinylated 137 000 and 113 000 Da proteins, we also observe a band with apparent molecular mass of 257 kDa in the erythrocyte ghost membranes both prior to and after the addition and photoactivation of exogenous Bz-CaM to the erythrocyte ghost membranes (data not shown). However, the densitometric analysis of the gel indicates that the relative intensity associated with the 257 kDa bands does not change when Bz-CaM is cross-linked to proteins associated with the erythrocyte ghost membrane. Therefore, it is apparent that the 257 kDa protein is another endogenous biotinylated protein present in the erythrocyte ghost membranes. We observe no cross-linked product between Bz-CaM and spectrin, in agreement with earlier results that indicate CaM does not normally associate with spectrin in mammalian erythrocyte membranes (Repasky & Gregorio, 1992). However, it should be mentioned that spectrin associated with avian erythrocytes and other mammalian tissues, and the β-isoform of spectrin in the denatured

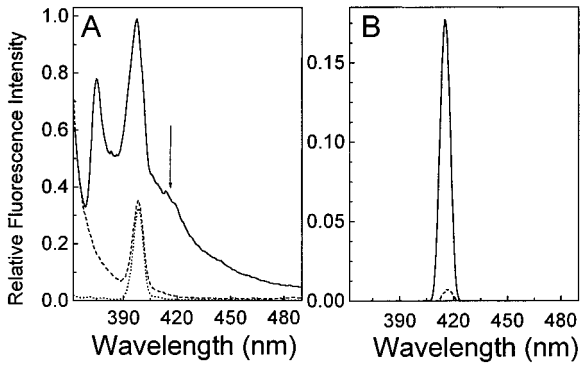

FIGURE 4: Fluorescence emission spectra associated with PMal-CaM bound to the PM-Ca-ATPase in native erythrocyte ghost membranes. Spectra were acquired in the absence (A) or presence (B) of the combination of a Schott GG400 long-pass filter together with an Oriel band-pass filter centered at 420 nm (full width at half-maximum is 10 nm) and correspond to PMal-CaM saturated ghost membrane (solid line), ghost membranes (dashed line), and buffer A alone (dotted line). When applicable, the total ghost membrane protein concentration was 0.25 mg mL^{-1}, and unbound PMal-CaM was eliminated by centrifugation (see the Experimental Procedures). Excitation was 351 nm, and the sample temperature was 25 °C.

form from mammalian erythrocytes, are all able to bind CaM (Repasky & Gregorio, 1992). Therefore, differences in both the animal source, tissue, and tertiary structure of spectrin can all influence CaM's binding properties.

Fluorescence Emission Spectra of PMal-CaM Bound to the Plasma Membrane Ca-ATPase. Having defined conditions that permit the selective association of CaM with the PM-Ca-ATPase, it is possible to address structural questions relating to the conformation and dynamics of CaM bound to the PM-Ca-ATPase. This task is complicated by the relatively small amount of CaM associated with the erythrocyte ghost membrane, resulting in a weak fluorescence signal. One does observe upon laser excitation of the PMal-CaM bound to the PM-Ca-ATPase on erythrocyte ghost membranes an emission spectrum characteristic of PMal-CaM with emission maxima centered at about 375 and 395 nm, and a broad shoulder centered at about 415 nm (Figure 4A). However, this spectrum contains substantial amounts of light scattering originating both from the suspension of erythrocyte ghost membranes and as a result of Raman scattering from the aqueous buffer centered at 398 nm, which account respectively for about 22% and 6% of the relative spectral intensity associated with PMal-CaM bound to the erythrocyte ghost membranes (Figure 4A). This level of light scattering will interfere with our ability to use frequency-domain fluorescence spectroscopy to resolve the structural properties of PMal-CaM bound to the PM-Ca-ATPase in erythrocyte ghost membranes. Therefore we have used a combination of two optical filters to minimize the contribution of light scattering to our measurement (Figure 4B). While the total integrated fluorescence signal associated with PMal-CaM is reduced about 27-fold relative to that observed in the absence of these filters, the interference due to scattered light is reduced about 250-fold. We are therefore in a position to measure the lifetime and rotational dynamics of PMal-CaM associated with the PM-Ca-ATPase in intact erythrocyte ghost membranes.

Measurement of the Fluorescence Lifetimes of PMal-CaM Bound to the Plasma Membrane Ca-ATPase. PMal-CaM was added to erythrocyte ghost membranes, and unbound

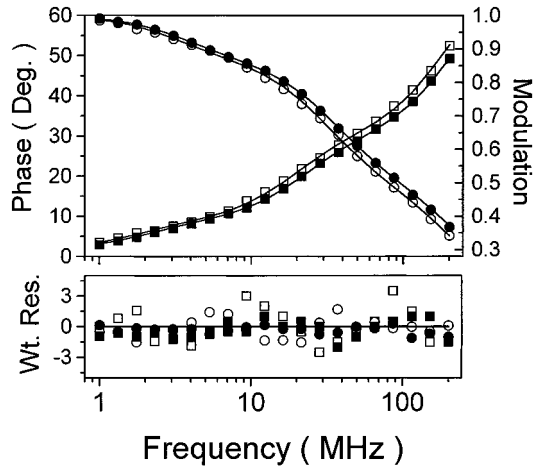

FIGURE 5: Frequency-domain fluorescence lifetime data of donor and donor−acceptor labeled CaM bound to erythrocyte ghost membranes. The frequency response of the phase shift (□, ■) and demodulation (○, ●) for *N*-(1-pyrenyl)maleimide labeled CaM (i.e., donor only; □, ○) and for *N*-(1-pyrenyl)maleimide labeled CaM in the presence of nitrotyrosine$_{139}$ (i.e., donor−acceptor; ■, ●). Symbols represent the experimental data, and solid lines represent the best fit to the data, as described in the Experimental Procedures. The goodness of fit was assessed both by the χ_R^2 and by the weighted residuals which correspond to the difference between the experimental data and the experimental fit normalized by the experimental error associated with the phase (i.e., $\delta_{phase} = 0.2°$) and modulation (i.e., $\delta_{modulation} = 0.005$). In all cases, measurements were made in buffer A at 25 °C using a ghost membrane protein concentration of 0.25 mg mL^{-1}, and samples were prepared as described in the Experimental Procedures.

CaM was removed (see above), permitting us to use frequency-domain fluorescence spectroscopy to measure the lifetime and to thereby assess the structure of CaM bound to the PM-Ca-ATPase in native erythrocyte ghost membranes. The phase lag and demodulation of intensity-modulated light were measured at 20 frequencies between 1 and 200 MHz for PMal-CaM in the presence of saturating amounts of calcium and native erythrocyte ghost membrane Ca-ATPase (Figure 5). The erythrocyte ghost membrane concentration was maintained at 0.25 mg mL^{-1} to both minimize light scattering and maintain sufficient signal for the fluorescence measurements. The intensity decay of PMal-CaM can be adequately described as a sum of three exponentials, as indicated by the random distribution of the weighted residues (Figure 5). There was a greater than 8-fold improvement in the goodness of fit (i.e., χ_R^2) for a model involving three exponentials relative to the two-exponential model (Table 1), further indicating that a model involving three exponentials is statistically justifiable. Inclusion of additional parameters results in no further improvement of χ_R^2.

The average fluorescence lifetime of PMal-CaM complexed with the PM-Ca-ATPase in native erythrocyte ghost membranes ($\bar{\tau} = 1.7 \pm 0.2$ ns, Table 1) is much smaller than that observed when PMal-CaM is complexed with the peptide C25W ($\bar{\tau} = 5.3 \pm 0.3$ ns, Table 1), which has an identical sequence to the CaM-binding sequence of the PM-Ca-ATPase. The shorter average lifetime observed for PMal-CaM in association with the PM-Ca-ATPase relative to that observed when CaM is complexed to C25W indicates that the local environment around the PMal located at Cys$_{27}$ on CaM is substantially different upon the association of CaM with the PM-Ca-ATPase in erythrocyte ghost membranes

Table 1: Lifetime Data For PMal-CaM in the Presence and Absence of Nitrotyrosine[a]

sample	α_1	τ_1 (ns)	α_2	τ_2 (ns)	α_3	τ_3 (ns)	$\bar{\tau}$ (ns)[b]	χ_R^{2} [c]
PMal-CaM + erythrocyte ghosts[d]	0.86 (0.02)	0.85 (0.06)	0.130 (0.005)	5.8 (0.2)	0.005 (0.001)	52 (4)	1.7 (0.2)	2.2 (18.9)
PMal-TNM-CaM + erythrocyte ghosts[d]	0.87 (0.02)	0.74 (0.04)	0.125 (0.003)	5.0 (0.2)	0.005 (0.001)	43 (1)	1.5 (0.2)	0.8 (8.9)
PMal-CaM + C25W[e]	0.78 (0.01)	2.14 (0.08)	0.200 (0.008)	9.8 (0.4)	0.016 (0.001)	104 (4)	5.3 (0.3)	0.7 (7.9)
PMal-TNM-CaM+ C25W[e]	0.78 (0.02)	1.54 (0.06)	0.200 (0.007)	7.3 (0.3)	0.016 (0.001)	77 (5)	3.9 (0.2)	1.3 (11.9)

[a] Average amplitudes (α_i) and lifetimes (τ_i) obtained from three-exponential fits to frequency-domain data collected for donor only (PMal-CaM) and donor−acceptor (PMal-TNM-CaM) labeled CaM. Uncertainties (in parentheses) represent the maximal variance associated with a rigorous analysis of the correlated errors between the five fitting parameters relative to the parameter of interest, as previously described (Beechem et al., 1991; Yao et al., 1994). [b] Average lifetime ($\bar{\tau}$) is calculated as: $\bar{\tau} = \Sigma\alpha_i\tau_i$, and is proportional to the quantum yield (Luedtke et al., 1981). Errors were propagated as described in Bevington (1969). [c] χ_R^2 for a two-exponential fit to the data is shown in parentheses. [d] Experimental conditions were identical to those described in the legend of Figure 5. [e] From Yao and Squier, (1996).

Table 2: Stern−Volmer Quenching Constants

sample	K_{sv} (M^{-1})[b]	$\bar{\tau}$ (ns)[b]	k_q (M^{-1} s^{-1})[c]	$k_q/k_{q(PMal-Cys)}$[d]
PMal-Cys[a]	385.1 ± 0.3	3.9 ± 0.2	$(9.9 \pm 0.5) \times 10^{10}$	1.0 ± 0.07
PMal-CaM + erythrocyte ghosts[e]	70.0 ± 0.1	1.7 ± 0.2	$(4.1 \pm 0.5) \times 10^{10}$	0.42 ± 0.05
PMal-CaM + C25W[f]	206.6 ± 0.4	5.3 ± 0.3	$(3.9 \pm 0.2) \times 10^{10}$	0.40 ± 0.03

[a] PMal-Cys is used to obtain a maximal value for the bimolecular quenching constant in the absence of steric influences relating to the tertiary structure of the protein. [b] K_{sv} is the Stern−Volmer quenching constant, and $\bar{\tau}$ is the average lifetime (see Table 1). [c] $k_q \equiv K_{sv}/\bar{\tau}$, and is the bimolecular quenching constant. [d] The quenching efficiency of PMal-CaM was normalized to that of PMal-Cys. [e] Experimental conditions were as described in the legend to Figure 5. [f] From Yao et al. (1996).

relative to that observed when CaM associates with C25W, and may be related to additional contact or electrostatic interactions between CaM and the PM-Ca-ATPase. The large decrease in the average fluorescence lifetime of PMal-CaM bound to the PM-Ca-ATPase relative to the average fluorescence lifetime of PMal-CaM bound to C25W is consistent with (i) our previous measurements that indicate that the observed lifetime of PMal-CaM complexed to a series of peptides that are identical to the primary sequence of the CaM-binding sequence in a series of target proteins is highly dependent on the structure and electrostatic properties of the neighboring amino acids adjacent to the CaM-binding sequence (Yao & Squier, 1996), and (ii) the large charge density associated with the sequence of the PM-Ca-ATPase's autoinhibitory domain adjacent to the carboxyl-terminal binding sequence for CaM (approximately 22% of the residues are acidic amino acids). Therefore, it is possible that either the sequence of the PM-Ca-ATPase adjacent to the CaM binding site or aspects of the tertiary structure of the PM-Ca-ATPase modify the conformational properties of the bound CaM. The modulation of the conformation of CaM bound to the PM-Ca-ATPase by the primary structure of the PM-Ca-ATPase has important implications with respect to the regulation of the PM-Ca-ATPase, since much of the isoform diversity associated with the PM-Ca-ATPase involves alterations in the carboxyl-terminal domain of the PM-Ca-ATPase near the CaM-binding sequence (reviewed by Carafoli et al., 1992; Stauffer et al., 1993).

Solvent Accessibility of N-(1-Pyrenyl)maleimide on CaM Bound to the PM-Ca-ATPase. The decrease in the average lifetime of PMal-CaM bound to the PM-Ca-ATPase relative to PMal-CaM bound to C25W may also be related only to the modification of the excited state properties of pyrene (Lakowicz, 1983; Schöneich et al., 1995). In order to better define possible conformational differences between PMal-CaM bound to the PM-Ca-ATPase in erythrocyte ghost membranes relative to PMal-CaM complexed to the peptide C25W, we have measured the solvent accessibility of PMal to the collisional quencher TEMPAMINE, as described in the Experimental Procedures. While we do observe significant differences in the Stern−Volmer quenching constant for PMal-CaM bound to erythrocyte ghosts relative to PMal-CaM bound to C25W (Table 2), the much larger Stern−Volmer quenching constant associated with CaM complexed to C25W ($K = 206.6 \pm 0.4$ M^{-1}) relative to CaM bound to the PM-Ca-ATPase in erythrocyte ghost membranes ($K = 70.0 \pm 0.1$ M^{-1}) is the result of the much larger average lifetime of PMal-CaM bound to C25W ($\bar{\tau} = 5.3 \pm 0.3$ ns, Table 1) relative to the average lifetime of PMal-CaM bound to the PM-Ca-ATPase ($\bar{\tau} = 1.7 \pm 0.2$ ns, Table 1). If one corrects for differences in the average lifetime, one finds that the bimolecular collisional quenching constant between TEMPAMINE and PMal-CaM bound to either C25W (i.e., $k_q = (3.9 \pm 0.2) \times 10^{10}$ M^{-1} s^{-1}) or the PM-Ca-ATPase (i.e., $k_q = (4.1 \pm 0.5) \times 10^{10}$ M^{-1} s^{-1}) are virtually identical (Table 2), indicating that the structural environment surrounding PMal is similar for PMal-CaM bound to either C25W or the PM-Ca-ATPase in erythrocyte ghost membranes. The similar collisional rate constants for CaM bound to either C25W or the PM-Ca-ATPase is in contrast to substantial alterations associated with the bimolecular collisional rate constant observed between TEMPAMINE and PMal-CaM bound to different target peptides derived from the CaM-binding sequence of a range of CaM-activatable proteins (Yao & Squier, 1996). Therefore, it is apparent that the primary structure of the CaM binding sequence on the PM-Ca-ATPase directly modulates the tertiary structure of the bound CaM, and that the conformation of CaM bound to the PM-Ca-ATPase is not modified by potential interactions with other aspects of the PM-Ca-ATPase sequence.

Spatial Separation between Globular Domains of CaM Bound to the PM-Ca-ATPase. In order to quantitatively assess the conformational changes associated with CaM binding to the native erythrocyte ghost membrane Ca-ATPase, we have used frequency-domain fluorescence spectroscopy to measure the FRET between PMal located at Cys_{27} and $nitrotyrosine_{139}$, providing a direct assessment of the average spatial separation between the opposing

Table 3: Spatial Separation between Chromophores on Opposing Globular Domains of CaM

sample	E (%)[a]	R_0 (Å)[b]	r_{app} (Å)[c]	R_{av} (Å)[d]	HW (Å)[d]	χ_R^2
CaM + erythrocyte ghosts[e]	15 (2)	14.7 (0.2)	19.6 (0.7)	20.2 (0.4)	8.6 (2.2)	2.1
CaM + C25W[f]	27 (2)	17.6 (0.2)	20.8 (0.2)	20.9 (0.3)	8.5 (1.3)	1.6

[a] Energy-transfer efficiency is obtained from changes in the average fluorescence lifetime ($\bar{\tau}$) of PMal-CaM upon nitration of Tyr_{139}, where $E = (1 - \bar{\tau}_{da} / \bar{\tau}_d)$ and is multipled by 100. Errors are the standard deviation of the mean. [b] The Förster critical distance (R_0) represents the distance between a given donor−acceptor pair under a given set of experimental conditions where the energy-transfer efficiency is 50% (Stryer, 1978). Indicated errors (in parentheses) represent the standard deviation of the mean. [c] Apparent donor−acceptor separation assuming a single unique protein conformation, as previously described (Yao et al., 1994), where the indicated errors are propagated (Bevington, 1969). [d] Average donor−acceptor separation (R_{av}) and associated full width at half-height (HW) assuming a Gaussian distribution of distances, where indicated errors (in parentheses) represent the maximal variance associated with a rigorous analysis of the error surfaces associated with each experimental parameter (Beechem et al., 1991). [e] Experimental conditions are as described in the legend in Figure 5. [f] From Yao and Squier (1996).

globular domains of CaM upon complexation with the PM-Ca-ATPase (Yao et al., 1994). In the presence of nitrotyrosine$_{139}$, we observe that the frequency response of PMal-CaM shifts toward higher frequencies (compare closed symbols to open symbols in Figure 5), consistent with the observed decrease in the average lifetime of PMal-CaM due to the presence of FRET to the acceptor nitrotyrosine$_{139}$ (Table 1). The intensity decay of PMal-nitrotyrosine$_{139}$-CaM is adequately described as a sum of three exponentials, as indicated by the random distribution of the weighted residues and the 11-fold improvement in χ_R^2 relative to a two-exponential model (Figure 5; Table 1).

A consideration of the Förster critical distance (R_0) under the conditions of interest in conjunction with the assessment of the average lifetime of PMal-CaM in the presence and absence of nitrotyrosine$_{139}$ (Table 1) permits us to measure the apparent donor−acceptor separation (r_{app}), which neglects any conformational heterogeneity in CaM by assuming a single donor−acceptor distance (Cheung, 1991). We observe very similar average distances between PMal located at Cys_{27} and nitrotyrosine$_{139}$ located on the opposing globular domains of CaM irrespective of whether CaM is bound to the PM-Ca-ATPase in erythrocyte ghost membranes ($r_{app} = 19.6 \pm 0.7$ Å; Table 3) or to the peptide C25W ($r_{app} = 20.8 \pm 0.2$ Å; Table 3).

Resolution of Conformational Heterogeneity of CaM Bound to the Erythrocyte Ghost Membrane Ca-ATPase. The frequency-domain intensity decays of PMal-CaM in the absence (donor only) and presence of nitrotyrosine$_{139}$ (donor−acceptor pair) were used to recover the time-dependent terms relating to the distribution of the donor−acceptor distances, permitting a measurement of the conformational heterogeneity between the opposing globular domains of CaM bound to the CaM binding sequence on the PM-Ca-ATPase (Haas et al., 1978; Lakowicz et al., 1988; Beechem & Haas, 1989; James et al., 1992; Yao et al., 1994; Yao & Squier, 1996). The average donor−acceptor separation ($r_{av} = 20.2$ Å; Table 3) is very similar to the apparent donor−acceptor separation calculated assuming a single unique conformation of CaM bound to the PM-Ca-ATPase ($r_{app} = 19.6 \pm 0.7$ Å; Table 3). The width of the donor−acceptor separation between the opposing globular domains is related to the conformational heterogeneity of CaM bound to the PM-Ca-ATPase and is the result of both the range of bound conformations of CaM associated with the PM-Ca-ATPase and the inherent flexibility of the CaM binding sequence. The observed HW (full width at half-maximum height) of the donor−acceptor distance distribution of CaM bound to the PM-Ca-ATPase is 8.6 ± 2.2 Å and is virtually identical to the width of the donor−acceptor distance distribution for CaM bound to C25W (i.e., 8.5 ± 1.3 Å; Table 3). The observed half-width is significantly narrower than the half-width of the distance distribution for either calcium saturated CaM (i.e., ∼12 Å) or apocalmodulin (i.e., ∼20 Å; Yao et al., 1994), indicating that there is less conformational heterogeneity between the opposing globular domains of CaM when complexed with either C25W or the PM-Ca-ATPase. The similar average distance and conformational heterogeneity of CaM bound to C25W and the PM-Ca-ATPase indicates that CaM binds to the PM-Ca-ATPase and C25W in a similar conformation, and that the conformational dynamics of the CaM binding site on the PM-Ca-ATPase are relatively unconstrained by the surrounding autoinhibitory sequence. Furthermore, these results provide strong evidence that the structural properties of CaM bound to a target peptide that is identical to the CaM-binding sequence on the PM-Ca-ATPase and CaM bound to the PM-Ca-ATPase in native erythrocyte ghost membranes are virtually identical.

Rotational Dynamics of CaM Bound to the Erythrocyte Ghost Membrane PM-Ca-ATPase. In order to further assess the structural properties of both CaM and the associated autoinhibitory domain of the PM-Ca-ATPase, we have measured the rotational dynamics of CaM in association with the PM-Ca-ATPase using frequency-domain fluorescence anisotropy. These measurements resolve both the segmental rotational motion associated with PMal at Cys_{27} on CaM and the overall rate of rotational motion of CaM associated with the PM-Ca-ATPase. The rate of segmental rotational motion is related to the steric hindrance around the chromophore and provides complementary information to the solvent accessibility data (Table 2), while the overall rate of rotational motion associated with the complex between CaM and the PM-Ca-ATPase provides information relating to the hydrodynamic properties of the autoinhibitory domain of the PM-Ca-ATPase.

In order to determine the rate of rotational motion for PMal-CaM associated with either the PM-Ca-ATPase or the C25W peptide, we measured the differential phase for PMal-CaM associated with these targets over 24 frequencies between 0.5 and 200 MHz (Figure 6). One observes that there is a continuous increase in the differential phase as the modulation frequency is increased, and that there is a substantial difference in the frequency response of the differential phase for calcium saturated CaM complexed with PM-Ca-ATPase relative to CaM bound to C25W. Furthermore, one observes that the steady-state polarization associated with PMal-CaM bound to the PM-Ca-ATPase ($P = 0.337 \pm 0.003$) is substantially higher than that of PMal-CaM in association with C25W ($P = 0.138 \pm 0.002$), suggesting that the rate of rotational motion occurring during

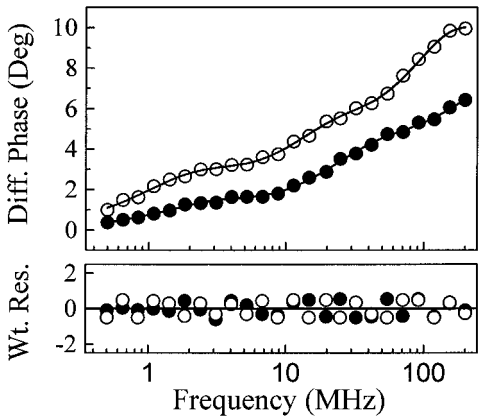

FIGURE 6: Rotational dynamics of *N*-(1-pyrenyl)maleimide labeled CaM bound to the PM-Ca-ATPase in erythrocyte ghost membranes. Frequency dependence of the differential phase for PMal-CaM bound to the PM-Ca-ATPase in erythrocyte ghost membranes (●) or to C25W (○). The weighted residuals (Wt. Res.) represent the difference between experimental and calculated values normalized by the assumed experimental error (i.e., 0.2°). Experimental conditions are as described in the legend to Figure 5, except that, in the case of PMal-CaM in association with C25W, the concentrations of CaM and C25W were 1.2 and 3.6 μM, respectively.

the excited state lifetime of PMal for CaM bound to the PM-Ca-ATPase is substantially less than that of PMal-CaM bound to C25W.

The frequency-domain anisotropy data obtained for PMal-CaM in association with either the PM-Ca-ATPase or C25W requires two exponentials to adequately describe the data, as is evidenced by the evenly distributed weighted residuals (Figure 6) and the greater than 12-fold reduction in the goodness of the fit (χ_R^2) relative to the one-exponential model (Table 4). Inclusion of additional fitting parameters results in no significant improvement in the calculated fit to the data. The amplitude (g_1r_0) and rate ($1/\phi_1$) of rotational motion associated with the segmental motion of PMal-CaM bound to the PM-Ca-ATPase ($g_ir_0 = 0.18 \pm 0.01$; $\phi_1 \sim 0.8 \pm 0.1$ ns) are essentially the same as those of CaM bound to C25W ($g_1r_0 = 0.17 \pm 0.01$; $\phi_1 \sim 0.9 \pm 0.1$ ns; Table 4), suggesting that the conformation surrounding PMal at Cys_{27} is very similar when CaM binds to either the PM-Ca-ATPase or the peptide derived from its autoinhibitory domain (C25W). Therefore, in conjunction with the FRET measurements (discussed above), these results indicate that the two globular domains of calcium saturated PMal-CaM move into closer juxtaposition upon binding to either the erythrocyte ghost plasma membrane Ca-ATPase or C25W with a similar reduction in their associated conformational heterogeneity (Table 3). The observed variation in the lifetime of PMal-CaM in association with either the PM-Ca-ATPase ($\bar{\tau} = 1.7 \pm 0.3$ ns) or C25W ($\bar{\tau} = 5.3 \pm 0.3$ ns; Table 1) suggests that the differences in the average lifetime of PMal located at Cys_{27} on CaM are related to minor alterations in the polarity of the surrounding environment, and are not the result of structural differences in the tertiary conformation of CaM. The rotational correlation time associated with the overall rotational motion of CaM bound to the PM-Ca-ATPase ($\phi_2 \approx 83 \pm 14$ ns) is much longer than that observed when CaM is bound to C25W ($\phi_2 \approx 10.3 \pm 0.5$ ns; Table 4), indicating that CaM is both rigidly bound to the PM-Ca-ATPase and that the CaM-binding domain of the PM-Ca-ATPase contains considerable tertiary structure. The structural implications relating to the observed rotational correlation times are examined in more detail in the Discussion.

DISCUSSION

Summary of Results. In order to assess the mechanisms associated with the ability of CaM to activate the PM-Ca-ATPase, we have used a fluorescent analog of wheat germ CaM to investigate the structural properties of CaM bound to the PM-Ca-ATPase in intact erythrocyte ghost membranes. The specific binding of one molecule of CaM to one PM-Ca-ATPase polypeptide chain in erythrocyte ghost membranes was established through the use of a photoactivatable cross-linking reagent conjugated to the single cysteine on CaM (i.e., Bz-CaM). Immunoblots using antibodies specific for both CaM and the erythrocyte PM-Ca-ATPase permit the identification of specific cross-linked products between CaM and the PM-Ca-ATPase (Figure 3). Structural measurements involving frequency-domain fluorescence spectroscopy were used to measure both the spatial separation and conformational heterogeneity between the opposing globular domains of CaM (Table 3) and the overall hydrodynamic properties of CaM bound to the CaM-binding domain of the PM-Ca-ATPase through the measurement of the overall rotational motion (Table 4, Figure 6). In addition, we have been able to assess more subtle conformational differences in CaM bound to either the entire PM-Ca-ATPase or the C25W peptide using fluorescence measurements of the lifetime (Table 1), segmental rotational dynamics (Table 4), and collisional quenching (Table 2) of PMal located at Cys_{27} on wheat germ CaM.

The average lifetime ($\bar{\tau}$) for PMal-CaM bound to the PM-Ca-ATPase in native erythrocyte ghost membranes ($\bar{\tau} = 1.7 \pm 0.2$ ns) is substantially shorter relative to that of PMal-CaM bound to C25W ($\bar{\tau} = 5.3 \pm 0.3$ ns), indicating a substantially greater polarity in the vicinity of Cys_{27} when CaM is bound to the PM-Ca-ATPase (Lakowicz, 1983; Schöneich et al., 1995). The observed difference in $\bar{\tau}$ is not the result of significant differences in the tertiary structure of CaM bound to the PM-Ca-ATPase relative to C25W, since we find (i) that CaM has a similar average spatial separation and distance distribution between PMal located at Cys_{27} in calcium binding loop I and nitrotyrosine$_{139}$ located in calcium binding loop IV (Figure 1; Table 3), (ii) that CaM has a similar solvent accessibility for PMal to collisional quenchers (Table 2), and (iii) that PMal undergoes a similar rate of segmental rotational dynamics (Table 4). Rather these differences in $\bar{\tau}$ reflect the much greater charge density near the PMal on CaM bound to the PM-Ca-ATPase, which may include the cluster of acidic residues adjacent to the CaM-binding sequence of the PM-Ca-ATPase (Strehler et al., 1990). The very similar structure of CaM bound to either the PM-Ca-ATPase or C25W indicates that (i) peptides with sequence identity to the CaM-binding domain of the PM-Ca-ATPase provide a realistic depiction of the structural properties of both CaM bound to the PM-Ca-ATPase and the associated secondary structure of the binding sequence on the PM-Ca-ATPase and (ii) the CaM binding sequence on the PM-Ca-ATPase is a contiguous sequence of amino acids within the primary structure of the PM-Ca-ATPase that is identical to C25W.

Since CaM is tightly associated with the CaM binding site on the autoinhibitory domain of the PM-Ca-ATPase, it is

Table 4: Rotational Dynamics of PMal-CaM[a]

sample	P[b]	g_1r_0[c]	ϕ_1 (ns)[c]	g_2r_0[c]	ϕ_2 (ns)[c]	χ_R^2 [d]
CaM + erythrocyte ghosts[e]	0.337 (0.003)	0.18 (0.01)	0.8 (0.1)	0.09 (0.01)	83 (14)	0.71 (8.7)
CaM +C25W[f]	0.138 (0.002)	0.17 (0.01)	0.9 (0.1)	0.10 (0.01)	10.3 (0.5)	0.78 (10.4)

[a] Reported correlation times and associated amplitudes were obtained from a multiexponential fit to the differential phase data, as described in the Experimental Procedures. [b] P is the steady-state polarization. [c] g_ir_0 are the amplitudes of the total anisotropy associated with each rotational correlation time (ϕ_i), where ϕ_1 and ϕ_2 are the rotational correlation times associated with segmental and overall rotational motion of CaM. Indicated errors were obtained from a rigorous consideration of the errors and account for all correlations between the measured parameters (Beechem et al., 1991; Yao et al., 1994), where the reported uncertainty is obtained using the F statistic and represents the maximal variance associated with one standard deviation relative to the reported values. [d] χ_R^2 describes the deviations between the model and experimental data, and the number in parentheses represents the χ_R^2 obtained from a one-component fit to the data. [e] Experimental conditions are described in the legend of Figure 5. [f] Data taken from Yao et al. (1996).

possible to measure the dynamic properties of CaM complexed to the PM-Ca-ATPase. We find that (i) there is no residual motional anisotropy and (ii) the overall rotational correlation time of the PMal-CaM bound to the PM-Ca-ATPase is much slower ($\phi_2 = 83 \pm 14$ ns; Table 4) than observed when CaM binds C25W ($\phi_2 = 10.3 \pm 0.5$ ns; Table 4). The lack of residual anisotropy indicates that PMal-CaM undergoes essentially isotropic rotational motion. The overall rotational correlation time associated with PMal-CaM bound to either the PM-Ca-ATPase or C25W is consistent with the tight binding of CaM. However, the rate of rotational motion is much faster than the corresponding rate of overall rotational motion associated with integral membrane proteins, which occurs on the time scale of tens of microseconds (Thomas et al., 1985; Cherry, 1992; Birmachu & Thomas, 1990; Birmachu et al., 1993). Therefore, the relatively rapid rotational dynamics of the CaM-binding domain relative to the overall rotational dynamics of the PM-Ca-ATPase and the absence of any residual anisotropy indicate that the autoinhibitory domain on the PM-Ca-ATPase undergoes large amplitude fluctuations during the excited state lifetime of PMal-CaM (i.e., $\bar{\tau} = 1.7 \pm 0.2$ ns). Thus, the CaM-binding domain is not undergoing significant inter- or intradomain stabilizing interactions with other portions of the PM-Ca-ATPase when CaM is bound.

Calculation of the Hydrodynamic Properties of the Autoinhibitory Domain of the PM-Ca-ATPase Complexed to CaM. The expected rotational correlation times for proteins of variable shape has been discussed in detail (Garcia de la Torre & Bloomfield, 1981; reviewed by Steiner, 1991), and coupled with some knowledge of the primary structure of a protein, it is possible to use the rate information from our frequency-domain anisotropy measurements for CaM bound to the PM-Ca-ATPase in erythrocyte ghost membranes to obtain structural information relating to the overall shape of the CaM-binding domain of the PM-Ca-ATPase. It is therefore useful to consider the known structural features associated with the autoinhibitory domain of the PM-Ca-ATPase subsequent to CaM binding in order to better understand the structural implications associated with the observed rotational correlation time of PMal-CaM bound to the PM-Ca-ATPase ($\phi_2 = 83 \pm 14$ ns; Table 4). For purposes of our discussion, we will emphasize the primary sequence of PMCA4, which is the dominant isoform in erythrocyte ghost membranes (Stauffer et al., 1995). The autoinhibitory domain of PMCA4 contains about 150 amino acids located on the carboxyl-terminal side of the tenth transmembrane sequence of the PM-Ca-ATPase (Figure 7). The autoinhibitory domain is delimited by a sequence that is especially prone to tryptic cleavage ($IPTR_{1052}$), which is predicted to be disordered and highly flexible (Zurini et al., 1984). There are 37 amino acids between this flexible linker and the CaM-binding sequence, which has been predicted to have a strong propensity to form an amphipathic α-helical structure (Garnier, 1978; reviewed by Carafoli et al., 1992). The remaining 116 amino acids contained within the autoinhibitory domain are predicted to contain substantial amounts of secondary structure, but little is known about the overall tertiary structure. Assuming that the autoinhibitory domain (which has a mass of 16,862 daltons) with CaM bound can be represented as a helical stalk connected to a globular domain (Figure 7), it is possible to calculate the expected rotational correlation time (ϕ) of this complex using the interpolating function provided by Garcia de la Torre and Bloomfield (1981), where:

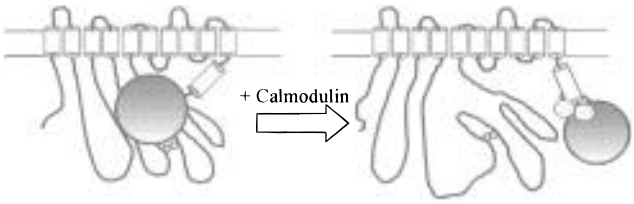

FIGURE 7: Model illustrating activation of the plasma membrane Ca-ATPase by CaM association. Structural cartoon depicting the relationship between the autoinhibitory domain of the PM-Ca-ATPase (large circle) before (left) and subsequent (right) to the binding of CaM (represented as two shaded circles connected by a flexible linker). The PM-Ca-ATPase is represented as containing ten putative transmembrane sequences and three major cytoplasmic domains. Sites associated with either phosphorylation (D475) or FITC binding (K609) are indicated as small circles and are generally thought to form part of the nucleotide binding site (Strehler et al., 1990). The CaM-binding site is adjacent to the autoinhibitory domain of the PM-Ca-ATPase and is located near the carboxyl-terminus. Prior to CaM binding, the autoinhibitory domain interacts with both major cytoplasmic domains of the PM-Ca-ATPase (Falchetto et al., 1992) and is presumed to block either access or utilization of substrates at the active site (reviewed by Carafoli, 1994). Subsequent to the association of CaM with the PM-Ca-ATPase, the autoinhibitory domain of the PM-Ca-ATPase both becomes dissociated from the nucleotide binding region and contains considerable tertiary structure. Under these conditions the associated calcium affinity of the PM-Ca-ATPase and maximal velocity are enhanced by about 7-fold (Figure 2).

$$D_r = \frac{kT}{8\pi\eta\sigma_1^3} \times \left(1 + \frac{L}{2\sigma_1}\right)^{-3} \times \left[1 + \sum_{i=1}^{3}\sum_{j=1}^{3} b_{ij}\left(1 - \left(1 + \frac{L}{2\sigma_1}\right)^{-1}\right)^i \times \left(\frac{\sigma_2}{\sigma_1}\right)^j\right]$$

D_r is the rotational diffusion coefficient relative to the

principal axis of the autoinhibitory domain, k is Boltzman's constant, η is the solvent viscosity (0.89 cP at 25 °C), T is the absolute temperature in K, L is the length of the stalk, σ_2 is the radius of stalk, and σ_1 is the radius of the globular domain complexed with CaM. The coefficients of the interpolating functions are $b_{11} = 3.886$, $b_{12} = 0.9412$, $b_{13} = 2.816$, $b_{21} = 4.546$, $b_{22} = 27.98$, $b_{23} = 6.335$, $b_{31} = 0.8185$, $b_{32} = 20.76$, and $b_{33} = -5.557$. In our calculation the length (L) of the stalk region is taken to be 55.5 Å based on secondary structure predictions for Ser_{1053} to Gly_{1109}, which is predicted to be α-helical (reviewed by Carafoli, 1994), and the hydrated radius of the stalk (σ_2) is assumed to be 3.8 Å. The hydrated radius (σ_1) of the globular domain (Gln_{1110} to Val_{1205} has a mass of 13,178 daltons) bound to PMal-CaM (which has a mass of 17,210) is 22.5 Å, assuming a spherical shape, a partial specific molar volume of 0.73 $cm^3\ g^{-1}$, and 30% hydration (Cantor & Schimmel, 1980). The calculated rotational diffusion coefficient is $2.5 \times 10^6\ s^{-1}$. Since:

$$\phi_c = \frac{1}{6 \times D_r}$$

the calculated rotational correlation time (ϕ_c) for the autoinhibitory domain of the PM-Ca-ATPase bound to CaM is about 68 ns. While ϕ_c is relatively insensitive to small changes in the length of the stalk region (for a 10 Å decrease in L there is a 15 ns decrease in ϕ_c), it is clear that the measured rotational correlation time associated with PMal-CaM bound to the PM-Ca-ATPase ($\phi_2 = 83 \pm 14$ ns; Table 4) is consistent with the general features of this model. Therefore, our measurements relating to the hydrodynamic properties of CaM bound to the PM-Ca-ATPase indicates that the complex between CaM and the autoinhibitory domain of the PM-Ca-ATPase forms a structurally distinct domain and that there are essentially no interactions between the autoinhibitory domain and other structural elements of the PM-Ca-ATPase. These results are consistent with earlier models in which the autoinhibitory domain of the PM-Ca-ATPase is predicted to be structurally distinct upon CaM association, and to undergo essentially no interactions with other structural elements of the PM-Ca-ATPase (Carafoli, 1994).

Alternative Models with Respect to the Structure of the Autoinhibitory Domain. High-resolution structural information is available for the the autoinhibitory domains of only two CaM-dependent enzymes (i.e., twitchin kinase and CaM-dependent protein kinase I; Hu et al., 1994; Goldberg et al., 1996), and there is no high-resolution information relating to the structural features of any autoinhibitory domain subsequent to CaM binding. However, the entire CaM-binding sequence is disordered in CaM-dependent protein kinase I, suggesting that the CaM-binding sequence does not undergo stabilizing interactions with other protein elements in either the catalytic core or within the autoinhibitory domain prior to CaM binding (Goldberg et al., 1996). If CaM bound to the PM-Ca-ATPase were to involve such a mobile structural element, ϕ_c would be about 10 ns (Yao & Squier, 1996). Likewise if one assumes (i) that the linker between Arg_{1052} and Gly_{1089} were disordered and mobile so as to uncouple the rotational dynamics of CaM bound to the autoinhibitory domain from the transmembrane structural elements of the PM-Ca-ATPase and (ii) that the complex between CaM and the autoinhibitory domain of the PM-Ca-ATPase could be approximated as a sphere, one can calculate that the expected rotational correlation time for CaM bound to the autoinhibitory domain of the PM-Ca-ATPase would be about 12 ns, which is much smaller than the observed rotational correlation time (see above). Assuming that the rotational dynamics of the autoinhibitory domain is uncoupled from the stalk, the calculated rotational correlation time approaches the observed rotational correlation time only if one assumes that the complex between CaM and the autoinhibitory domain of the PM-Ca-ATPase can be approximated as a rigid prolate ellipsoid with an axial ratio of about 20:1, corresponding to a minor radius of about 8.5 Å and a long axis of 170 Å. However, the latter structure is inconsistent with the dimensions of CaM bound to a range of target peptides (including C25W; Meador et al., 1993; Yao & Squier, 1996), whose minor axis should represent the minimal dimensions associated with the autoinhibitory domain of the PM-Ca-ATPase.

Other possible models associated with the activation of the PM-Ca-ATPase subsequent to CaM binding include the association of the autoinhibitory domains on adjacent PM-Ca-ATPase polypeptide chains, which has previously been shown to activate the PM-Ca-ATPase solubilized in detergent (Kosk-Kosicka & Bzdega, 1988; Vorherr et al., 1991). However, the activation of the PM-Ca-ATPase through the association of the autoinhibitory domains is competitive with respect to CaM binding (Sachett and Kosk-Kosicka, 1996) and is not consistent with 1:1 stoichiometry of CaM binding with the PM-Ca-ATPase in native erythrocyte ghost membranes (Figure 3). Therefore, the formation of oligomeric complexes between PM-Ca-ATPase polypeptide chains and the associated CaM-independent activation of the PM-Ca-ATPase in detergent is not physiologically relevant.

Relationship to Other Studies. Earlier experiments have demonstrated an ability to fully activate the PM-Ca-ATPase upon proteolytic cleavage of the CaM-binding domain, to restore CaM regulation upon the addition of peptides that are identical to the CaM-binding site on the PM-Ca-ATPase, and to cross-link these regulatory peptides to the transduction domains of the PM-Ca-ATPase (Benaim et al., 1984; Zurini et al., 1984; Wang et al., 1988; James et al., 1988; Enyedi et al., 1989; Falchetto et al., 1991, 1992). Our results demonstrate that, upon CaM binding, the autoinhibitory domain of the PM-Ca-ATPase is dissociated from the PM-Ca-ATPase, consistent with earlier suggestions that CaM binding to the PM-Ca-ATPase results in the removal of steric inhibition at the catalytic site of the PM-Ca-ATPase due to the dissociation of the autoinhibitory domain from the PM-Ca-ATPase (reviewed by Carafoli, 1994). While there are currently no direct measurements relating to the structure of the autoinhibitory domain of the PM-Ca-ATPase prior to CaM binding, there are multiple sites located in the CaM-binding domain that are especially prone to proteolytic cleavage by either trypsin or calpain (Carafoli et al., 1992). The susceptibility of the CaM binding site to proteolytic cleavage suggests that the CaM-binding site is both exposed and highly flexible prior to CaM binding, consistent with the structure of the CaM-binding sequence in CaM-dependent protein kinase I (Goldberg et al., 1996). Upon CaM binding, the autoinhibitory domain of the PM-Ca-ATPase undergoes essentially isotropic rotational motion as a rigid body (Figure 7; see above). Previous measurements indicate that, subse-

quent to their association with CaM, the structures of a wide range of peptides that are identical to the CaM-binding sequences of a variety of CaM-dependent target proteins assume an α-helical conformation (reviewed by Trewhella, 1992; Meador et al., 1992, 1993; Yao & Squier, 1996), and that the structures of CaM bound to C25W and the PM-Ca-ATPase are virtually identical (see above). Therefore, a disordered to ordered structural transition associated with the CaM-binding sequence of the PM-Ca-ATPase upon CaM binding may represent the trigger associated with the disruption of the stabilizing interactions between the autoinhibitory domain and other protein structural elements.

Conclusions and Future Directions. We report (i) that CaM specifically and selectively associates with the CaM-binding sequence on the autoinhibitory domain of the PM-Ca-ATPase in native porcine erythrocyte ghost membranes at a stoichiometry of one molecule of CaM bound to one PM-Ca-ATPase polypeptide chain, (ii) that the structural properties of CaM and the associated CaM-binding site on the PM-Ca-ATPase are virtually identical to the structural properties of CaM complexed with a peptide (i.e., C25W) that has an identical sequence to the CaM-binding site on the autoinhibitory domain of the PM-Ca-ATPase, and (iii) that the CaM-binding domain of the PM-Ca-ATPase undergoes essentially unrestricted rotational motion subsequent to CaM binding, providing direct evidence that CaM binding releases the inhibition associated with the autoinhibitory domain of the PM-Ca-ATPase through the dissociation of the autoinhibitory domain from the catalytic portion of the calcium pump. Our current measurements do not address the regulation of the PM-Ca-ATPase by the site-specific phosphorylation of residues associated with the autoinhibitory domain by protein kinase C and cAMP-dependent protein kinase, which may also modulate the interaction between the autoinhibitory domain and other structural elements in the PM-Ca-ATPase. Future studies will emphasize additional regulatory mechanisms associated with post-translational modifications involving site-specific oxidative modifications and phosphoryl group transfer reactions to both CaM and the autoinhibitory domain of the PM-Ca-ATPase (James et al., 1988, 1989; Wang et al., 1991; Rodin et al., 1992; Yao et al., 1996), and their relationship to the structure of the autoinhibitory domain of the PM-Ca-ATPase.

ACKNOWLEDGMENT

We wish to thank Drs. Adelaida Filoteo and John Penniston for providing the monoclonal Ca-ATPase antibody 5F10 antibody used in this study, Gouri S. Jas for his assistance in preparing the structural cartoon of CaM, Diana J. Bigelow for many helpful discussions, and Christian Schöneich for making his Rayonet photoreactor available for our cross-linking studies.

REFERENCES

Adamo, H. P., Rega, A. F., & Garrahan, P. J. (1990) *J. Biol. Chem. 265*, 3789−3792.

Adebayo, A. O., Enyedi, A., Verma, A. K., Filoteo, A. G., & Penniston, J. T. (1995) *J. Biol. Chem. 270*, 27812−27816.

Anderson, J. P., & Morrow, J. S. (1987) *J. Biol. Chem. 262*, 6365−6372.

Beechem, J. M., & Haas, E. (1989) *Biophys. J. 55*, 1225−1236.

Benaim, G., Zurini, M., & Carafoli, E. (1984) *J. Biol. Chem. 259*, 8471−8477.

Bevington, P. R. (1969) in *Data Reduction and Error Analysis for the Physical Sciences*, McGraw-Hill, New York.

Bewaji, C. O., & Bababunmi, E. A. (1987) *Biochem. J. 248*, 297−299.

Birmachu, W., & Thomas, D. D. (1990) *Biochemistry 29*, 3904−3914.

Birmachu, W., Voss, J. C., Louis, C. F., & Thomas, D. D. (1993) *Biochemistry 32*, 9445−9453.

Borke, J. L., Caride, A., Verma, A. K., Pennistion, J. T., & Kumar, R. (1989) *Am. J. Physiol. 257*, F842−F849.

Cantor, C. R., & Schimmel, P, R. (1980) *Biophysical Chemistry, Part II*: *Techniques for the study of biological structure and function*, pp 549−588, W. H. Freeman and Co., San Francisco.

Carafoli, E. (1992) *J. Biol. Chem. 267*, 2115−2118.

Carafoli, E. (1994) *FASEB J. 8*, 993−1002.

Carafoli, E., Kessler, F., Falchetto, R., Heim, R., Quadroni, M., Krebs, J., Strehler, E. E., & Vorherr, T. (1992) *Ann. N. Y. Acad. Sci. 671*, 58−69.

Chapman, E. R., Alexander, K., Vorherr, T., Carafoli, E., & Storm, D. R. (1992) *Biochemistry 31*, 12819−12825.

Chattopadhyaya, R., Meador, W. E., Means, A. R., & Quiocho, F. A. (1992) *J. Mol. Biol. 228*, 1177−1192.

Cherry, R. J. (1992) in *The Structure of Biological Membranes* (Yeagle, P., Ed.) pp 507−537, CRC Press, Boca Raton.

Cheung, W. Y. (1991) in *Topics in Fluorescence Spectroscopy* (Lakowicz, J. R., Ed.) Vol. 2, pp 128−176, Plenum Press, New York.

Crivici, A., & Ikura, M. (1995) *Annu. Rev. Biophys. Biomol. Struct. 24*, 85−116.

Dormán, G., & Prestwich, G. D. (1994) *Biochemistry 33*, 5661−5673.

Enyedi, A., Vorherr, T., James, P., McCormick, D. J., Filoteo, A. G., Carafoli, E., & Penniston, J. T. (1989) *J. Biol. Chem. 264*, 12313−12321.

Fabiato, A. (1988) *Methods Enzymol. 157*, 378−417.

Fabiato, A., & Fabiato, F. (1979) *J. Physiol. (Paris) 75*, 463−505.

Fairclough, R. H., & Cantor, C. R. (1978) *Methods Enzymol. 48*, 347−379.

Falchetto, R., Vorherr, T., Brunner, J., & Carafoli, E. (1991) *J. Biol. Chem. 266*, 2930−2936.

Falchetto, R., Vorherr, T., & Carafoli, E. (1992) *Protein Sci. 1*, 1613−1621.

Garcia de la Torr, J., & Bloomfield, V. (1981) *Q. Rev. Biophys. 14*, 81−139.

Garnier, J. (1978) *J. Mol. Biol. 120*, 97−120.

Goldberg, J., Nairn, A. C., & Kuriyan, J. (1996) *Cell 84*, 875−887.

Gopalakrishna, R., & Anderson, W. B. (1982) *Biochem. Biophys. Res. Commun. 104*, 830−836.

Gornal, A., Bardawill, C., & David, M. (1949) *J. Biol. Chem. 177*, 751−766.

Guerini, D., Foletti, D., Vellani, F., & Carafoli, E. (1996) *Biochemistry 35*, 3290−3296.

Haaker, H., & Racker, E. (1979) *J. Biol. Chem. 254*, 6598−6602.

Haas, E., Katchalski-Katzir, E., & Steinberg, I. (1978) *Biochemistry 17*, 5064−5070.

Hinds, T. R., & Andreasen, T. J. (1981) *J. Biol. Chem. 256*, 7877−7881.

Hu, S.-H., Parker, M. W., Lei, J. Y., Wilce, M. C. J., Benian, G. M., & Kemp, B. E. (1994) *Nature 369*, 581−584.

Husain, A., Howlett, G. J., & Sawyer, W. H. (1984) *Biochem. Biophys. Res. Commun. 122*, 1194−1200.

Inesi, G. (1994) *Biophys. J. 66*, 554−560.

Inesi, G., Cantilina, T., Yu, X., Nikic, D., Sagara, Y., & Kirtley, M. E. (1992) *Ann. N.Y. Acad. Sci. 671*, 32−48.

James, E., Wu, P. G., Stites, W., & Brand, L. (1992) *Biochemistry 31*, 10217−10225.

James, P., Maeda, M., Fischer, R., Verma, A. K., Krebs, J., Penniston, J. T., & Carafoli, E. (1988) *J. Biol. Chem. 263*, 2905−2910.

James, P., Pruschy, M., Vorherr, T., Penniston, J. T., & Carofolio, E. (1989) *Biochemistry 28*, 4253−4258.

James, P., Vorherr, T., & Carafoli, E. (1995) *Trends Biochem. Sci. 20*, 38−42.

Jarrett, H. W., & Penniston, J. T. (1977) *Biochem. Biophys. Res. Commun. 77*, 1210−1216.

Jarrett, H. W., & Kyte, J. (1979) *J. Biol. Chem. 254*, 8237−8244.
Johnson, M. L., & Faunt, L. M. (1992) *Methods Enzymol. 210*, 1−37.
Kessler, F., Falchetto, R., Hein, R., Meili, R., Vorherr, T., Strehler, E. E., & Carafoli, E. (1992) *Biochemistry 31*, 11785−11792.
Knauf, P. A., Proverbio, A. F., & Hoffman, J. F. (1974) *J. Gen. Physiol. 63*, 324−336.
Kosk-Kosicka, D., & Bzdega, T. (1988) *J. Biol. Chem. 263*, 18184−18189.
Kosk-Kosicka, D., & Bzdega, T. (1990) *Biochemistry 29*, 3773−3777.
Kosk-Kosicka, D., Bzdega, T., & Johnson, J. D. (1990) *Biochemistry 29*, 1875−1879.
Kraulis, P. J. (1991) *J. Appl. Crystallogr. 24*, 946−950.
Lakowicz, J. R. (1983) in *Principles of Fluorescence Spectroscopy*, Plenum Publishing Corp., New York.
Lakowicz, J. R., & Gryczynski, I. (1991) in *Topics in Fluorescence Spectroscopy* (Lakowicz, J. R., Ed.) Vol. I, pp 293−335, Plenum Press, New York.
Lakowicz, J. R., Cherek, H., Maliwal, B. P., & Gratton, E. (1985) *Biochemistry 24*, 376−383.
Lakowicz, J. R., Gryczynski, I., Cheung, H. C., Wang, C., Johnson, M. L., & Joshi, N. (1988) *Biochemistry 27*, 9149−9160.
Lakowicz, J. R., Gryczynski, I., Wiczk, W., Kuśba, J., & Johnson, M. L. (1991) *Anal. Biochem. 195*, 243−254.
Lanzetta, P. A., Alverez, L. J., Reinsch, P. S., & Candia, O. (1979) *Anal. Biochem. 100*, 95−97.
Lehrer, S. S., & Leavis, P. C. (1978) *Methods Enzymol. 49*, 222−236.
Luedtke, R., Owen, C. S., Vanderkooi, J. M., & Karush, F. (1981) *Biochemistry 20*, 2927−2936.
Matthews, J. C. (1993) *Fundamentals of Receptor, Enzyme, and Transport Kinetics*, CRC Press, Boca Raton.
Niggli, V., Penniston, J. T., & Carafoli, E. (1979) *J. Biol. Chem. 254*, 9955−9958.
Pederson, P. L., & Carafoli, E. (1987a) *Trends. Biochem. Sci. 12*, 146−150.
Pederson, P. L., & Carafoli, E. (1987b) *Trends. Biochem. Sci. 12*, 186−189.
Pedigo, S., & Shea, M. (1995) *Biochemistry 34*, 1179−1196.
Repasky, E. A., & Gregorio, C. C. (1992) in *The Structure of Biological Membranes* (Yeagle, P., Ed.) pp 449−505, CRC Press, Boca Raton.
Richman, P. G., & Klee, C. B. (1978) *Biochemistry 17*, 928−935.
Rodin, P., Falchetto, R., Vorherr, T., & Carofoli, E. (1992) *Eur. J. Biochem. 204*, 936−946.
Sackett, D. L., & Kosk-Kosicka, D. (1996) *J. Biol. Chem. 271*, 9987−9991.
Schöneich, Ch., Hühmer, A. F. R., Rabel, S. R., Stobaugh, J. F., Jois, S. D. S., Larive, C. K., Siahaan, T. J., Squier, T. C., Bigelow, D. J., & Williams, T. D. (1995) *Anal. Chem. 67*, 155R−181R.
Stauffer, T. P., Hilfiker, H., Carafoli, E., & Strehler, E. E. (1993) *J. Biol. Chem. 268*, 25993−26003.
Stauffer, T. P., Guerini, D., & Carafoli, E. (1995) *J. Biol. Chem. 270*, 12184−12190.
Steiner, R. F. (1991) in *Topics in Fluorescence Spectroscopy* (Lakowicz, J. R. Ed.) Vol. 2, pp 1−52, Plenum Press, New York.
Strasburg, G. M., Hogan, M., Birmachu, W., Thomas, D. D., & Louis, C. F. (1988) *J. Biol. Chem. 263*, 542−548.
Strehler, E. E., James, P., Fischer, R., Heim, R., Vorherr, T., Filoteo, A. G., Penniston, J. T., & Carofoli, E. (1990) *J. Biol. Chem. 265*, 2835−2842.
Stryer, L. (1978) *Annu. Rev. Biochem. 47*, 819−846.
Tao, T., Lamkin, M., & Scheiner, C. J. (1985) *Arch. Biochem. Biophys. 40*, 627−634.
Thomas, D. D., Eads, T. M., Barnett, V. A., Lindahl, K. M., Momont, D. M., & Squier, T. C. (1985) in *Spectroscopy and the Dynamics of Biological Systems* (Bailey, P. M., & Dale, R. E., Eds.) Academic Press, London.
Török, K., Lane, A. N., Martin, S. N., Janot, J.-M., & Bailey, P. M. (1992) *Biochemistry 31*, 3452−3462.
Vorherr, T., Kessler, T., Hofmann, F., & Carafoli, E. (1991) *J. Biol. Chem. 266*, 22−27.
Wang, K. K. W., Villalobo, A., & Roufogalis, B. D. (1988) *Arch. Biochem. Biophys. 260*, 696−704.
Wang, K. K. W., Wright, L. C., Madian, C. L., Allen, B. G., Conigrave, A. D., & Roufogalis, B. D. (1991) *J. Biol. Chem. 266*, 9078−9085.
Weber, G. (1981) *J. Phys. Chem. 85*, 949−953.
Yacko, M. A., Vanaman, T. C., & Butterfield, D. A. (1991) *Biochim. Biophys. Acta 1064*, 7−12.
Yao, Y., & Squier, T. C. (1996) *Biochemistry 35*, 6815−6827.
Yao, Y., Schöneich, Ch., & Squier, T. C. (1994) *Biochemistry 33*, 7797−7810.
Yao, Y., Yin, D., Jas G. S., Kuczera, K., Williams, T. D., Schöneich, Ch., & Squier, T. C. (1996) *Biochemistry 35*, 2767−2787.
Zurini, M., Krebs, J., Penniston, J. T., & Carafoli, E. (1984) *J. Biol. Chem. 259*, 618−627.

BI960834N